Taylor & Francis
Taylor & Francis Group

Cost-effective non-metric close-range digital photogrammetry and its application to a study of coarse gravel river beds*

PATRICE E. CARBONNEAU†,

Student, Université du Québec, INRS-Géoressources, 880 chemin Ste-Foy, CP 7500, GIV 4C7, Québec, Canada; e-mail: pcarbonn@nrcan.gc.ca

STUART N. LANE

School of Geography, University of Leeds, Leeds, UK

and NORMAND E. BERGERON

Université du Québec, INRS-Géoressources, Québec, Canada

Abstract. Digital photogrammetry is now increasingly recognized as being a powerful tool in geomorphology. However, the high material costs and skills required by digital photogrammetry may deter non-photogrammetrists from using this technique in their research. This paper demonstrates the use of a close-range digital photogrammetric methodology accessible to non-photogrammetrists and yet capable of yielding good quality topographic information on coarse gravel riverbeds at minimal cost. Digital Elevation Models (DEMs) were derived from 1:165 scale imagery obtained with a 35 mm film SLR camera, a commercial desktop scanner and a softcopy photogrammetry package. Quality assessment based upon independent checkpoints and scaling analysis showed that the precision of the DEMs was consistently less than 10% of the D_{50} of the bed particles. This translates into sub-centimetric precision. Whilst photogrammetry is presently capable of a better data quality at this scale, quality must be judged with respect to the requirements of the geomorphological applications under consideration. Thus, the methodological simplifications adopted in this research are acceptable in order to make photogrammetry both cost-effective and accessible.

1. Introduction

Digital elevation models (DEMs) are increasingly being used in fluvial geomorphology for modelling and monitoring riverbed structure. Recent work by Butler *et al.* (2001), Lane *et al.* (2000) and Stojic *et al.* (1998) demonstrates that close-range photogrammetry can produce high quality and high-density data allowing an investigation of the complex structures of riverbeds that has previously been impossible.

The research presented in this paper was initiated by a need to characterize the

---

*Contribution to the program of CIRSA (Centre Interuniversitaire de Recherche sur le Saumon Atlantique).

†Corresponding author.

gravel beds used as over-wintering habitat by juvenile Atlantic salmon (*salmo salar* L.). During winter days, the survival strategy of juvenile salmon involves concealment in the interstitial voidspaces of the bed (Rimmer *et al.* 1983, Cunjak 1988). While it is well established that the river reaches selected by Atlantic salmon for over-wintering are comprised of coarse gravel (Rimmer *et al.* 1983, Heggenes 1996), deeper understanding and modelling of interstitial habitat space is limited by a lack of methods for quantifying and describing the structure of coarse gravel beds and their interstitial voidspaces. Field observations strongly suggest that a relationship exists between the complexity of the bed and the available habitat space. Complexity was therefore hypothesized as being a parameter capable of quantifying the structure and available habitat space in gravel beds in a more explicit manner than conventional roughness measurements which do not take into account particle organization. Quantitative evaluation of surface complexity requires high resolution sampling of surface elevation (Butler *et al.* 2001). In this context, the digital photogrammetric methodology presented here was developed to obtain DEMs of appropriate resolution and quality for the quantification of surface complexity. The resolution and quality of the DEMs were established based on the habitat requirements of juvenile salmon.

Rimmer *et al.* (1983) showed that juvenile Atlantic salmon preferentially select their winter habitat near coarse particles ('home stones') having a mean diameter of approximately 20 cm. Gregory and Griffith (1996) examined the selection of artificial concealment spaces by subyearling rainbow trout and found that preferred spaces were those where the fish were able to set their pectoral fins on the riverbed while leaving the dorsal and caudal fins free to move. Considering the size and morphology of juvenile salmonids, suitable concealment spaces are therefore approximately of a few centimetres in size. For such a small scale, manual measurement of surface elevations with conventional surveying equipment followed by interpolation is not capable of yielding DEMs of sufficient resolution. This is why photogrammetry was selected. Suitable photogrammetric DEMs for this study should therefore be of sub-centimetric spatial resolution and precision. Thus, the aim of this paper is to assess the extent to which an accessible, cost-effective, close-range digital photogrammetric methodology is applicable to this scale of work.

2. Photogrammetric and analytical considerations

This section reviews the principles that make implementation of cost-effective photogrammetry possible and the concepts relevant to data quality, a topic that is too often forgotten (Lane *et al.* 2000).

2.1. *Hardware advances*

Use of digital imagery and advances in computer-related technologies have made the material requirements of digital photogrammetry less stringent than those of traditional analogue photogrammetry (Chandler and Padfield 1996, Chandler 1999). Experience of camera calibration procedures, such as the self-calibrating bundle adjustment, now make it possible for digital photogrammetry to be carried out with non-metric commercial 35 mm SLR cameras (either digital or film based) rather than with the traditional calibrated metric cameras (Short 1992, Fryer 1996). One such package, CUBA (City University Bundle Adjustment), is freely available on the World Wide Web (Short 1999). Thus, with effective calibration, use of 35 mm film cameras could potentially make photogrammetry much more cost effective. Digital

cameras also show much potential for digital photogrammetry (Ahmad and Chandler 1999). However, the current cost of 35 mm SLR digital cameras remains relatively high and thus defeats the cost-effectiveness objective of this work.

The use of 35 mm SLR cameras will predictably cause a certain loss of accuracy (Chandler and Padfield 1996). The key question that remains is whether or not this loss of accuracy is acceptable for a given application. This was answered in the affirmative for non-metric close-range analytical photogrammetry based on 35 mm camera imagery of streambed morphology (Welsh and Jordan 1983). If it also holds for digital photogrammetric applications, which must consider additional issues such as scanning and the effects of automated DEM extraction, then it allows for the replacement of traditionally expensive and specialized cameras by inexpensive, 'off the shelf' equipment. Softcopy photogrammetry packages, which replace the analogue stereo plotter, have a comparatively lower cost and are much easier to use (Chandler and Padfield 1996). Furthermore, these packages often offer an automated collection procedure that offers the possibility of easily generated high density DEMs.

2.2. *Implications of automated DEM generation for data quality*

Traditional photogrammetry relied on the user to identify conjugate points in a stereo pair in order to restitute the three-dimensional geometry of the object/landform under consideration. Manual DEM collection results in a time limit upon the total number of elevations that can be collected. Automated DEM collection procedures use pixel information to match conjugate points. The most commonly used matching procedure is area-based. Images patches, comprising a pixel submatrix from each image are cross-correlated. Conjugate point pairs, i.e. the location of a given object in both images, are identified as the highest pixel patch cross-correlation (Dowman 1996, Butler *et al.* 1998). Automation of the matching process greatly increases the density of DEMs that can be attained and, due to greater reliance upon software rather than expensive hardware, it also implies that the user no longer requires specialist equipment to extract DEMs, therefore opening the field of photogrammetry to non-photogrammetrists. However, this apparent ease of use must be treated with caution. The replacement of human judgement during matching introduces the potential of additional error. Matching errors take two forms, incorrect matches and unsuccessful matches. Incorrect matches occur when the algorithm identifies incorrect conjugate pairs. An unsuccessful match occurs when the algorithm fails completely to identify a conjugate pair for a given location. In the first case, the resulting elevation will be false. In the second, elevation will be interpolated, using a bilinear method, and the accuracy will depend on the effectiveness of the interpolation which is a function of surface structure (Lane *et al.* 2000).

A classic difficulty leading to either error is the perspective problem. During matching, the highest correlation will be achieved for two identical patches: an image of a given object should be identical in both images of the stereo pair for a perfect match to occur. However, photogrammetric restitution of an object's imagery is made possible by the fact that images are taken from different camera stations. In the case of three-dimensional objects, this creates differences in patch appearance on the two images that will be proportional to the ratio of the relative roughness in the image to the flying height of the camera (camera-object distance). In cases where this ratio is high, images along the edges of larger objects may in fact be quite different. Figure 1 shows an example, taken from a study site used in this research, where targets adjacent to a stone and visible in the right image are hidden by this
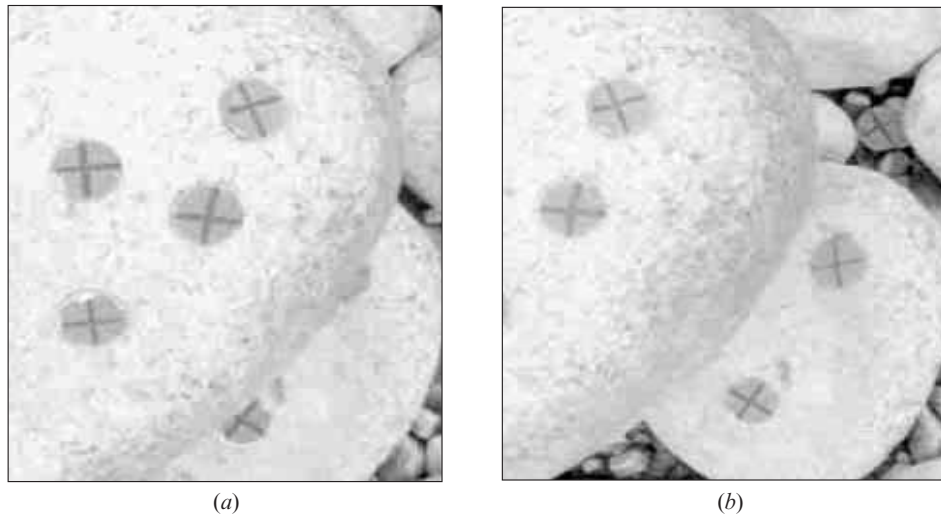
Figure 1.   Illustration of perspective error.

stone in the left image. These differences in images, common along edges, cause the matching algorithm to fail and are known as perspective errors. Perspective errors may cause incorrect matches if the algorithm is still able to find patches with sufficient correlation. Unsuccessful matches may also occur, leaving elevations to be determined by interpolation.

Thus, the transition to automated DEM generation introduces errors that must be assessed (Lane *et al.* 2001). Following engineering surveying practices, the data quality of a surface may be examined according to three aspects: random errors, systematic errors and external reliability (Cooper and Cross 1988, Butler *et al.* 1998, Lane *et al.* 2001). At the level of the surface, random errors are best represented by the standard deviation of all point errors (SDE). Systematic error is represented by the mean error (ME).

One difficulty of quality assessment is the acquisition of a sufficient number of independent survey data, also called check data, to properly represent the surface (Lane *et al.* 2000). Even when such data are available, accuracy statistics remain insensitive to changes in parameters used in the DEM collection algorithm (Lane *et al.* 2000). However, spatially distributed surface derivatives, such as slopes and aspects derived from the DEM, have been found to be sensitive to DEM collection parameters. Thus, they can be used in combination with check data for DEM quality assessment. Surface derivatives may be more reliable for quality assessment if they are insensitive to decisions made during data collection.

2.3. *Basis for external reliability analysis*

External reliability is evaluated by comparing a parameter derived from the DEM with a theoretical reference. In large-scale DEMs, external reliability can be based upon slope values (Lane *et al.* 2000) or other hydrologically relevant parameters (Walker and Willgoose 1999). However, this may be inappropriate for the small-scale DEMs of interest to this study. Recently, Lane *et al.* (2000) have compared DEM scaling properties to the expected scaling properties of natural surfaces as predicted by fractal theory (Russ 1994, Nikora *et al.* 1998). For natural surfaces,

scaling properties are studied by computing the variance of elevation differences as a function of scale. In geomorphology, the semivariogram is the most reliable tool for this analysis (Butler *et al.* 2001). Roberts (1988, 1991) and Bergeron (1998) both used the one-dimensional semivariogram to study roughness characteristics of linear topographic profiles of streambeds. Butler *et al.* (2001) have used two-dimensional semivariograms to study scaling properties of DEMs obtained with digital photogrammetry.

The two-dimensional semivariogram is given by (generalized from Butler *et al.* 2001):

$$\gamma(p,q) = \frac{1}{2(N-|p|)(M-|q|)} \sum_{i=1+|p|-p/2}^{N-|p|+p/2} \sum_{j=1+|q|-q/2}^{M-|q|+q/2} [Z(i+p, j+q) - Z(i,j)]^2 \quad (1)$$

where p and q are the lag components in the x and y directions, and M and N are the dimensions of the surface in the x and y directions respectively and $Z(i,j)$ is the elevation at point (i,j). The complex form of the summation indices is necessary for the computation of negative lags. Negative lags, meaningless in one-dimensional scaling analysis, are necessary in two-dimensional scaling analysis. The combinations of p, q should allow for measurement of semivariance along all orientations ($0°$ to $360°$) of the surface. The orientation at a given lag is:

$$\omega = \arctan\left(\frac{q}{p}\right) \quad (2)$$

If p and q are positive, only angles from $0°$ to $90°$ are covered, thus justifying the necessity to compute the semivariance for all combinations of $\pm p$ and $\pm q$. However, examination of equation (1) shows a symmetry where $\gamma(p,-q)=\gamma(-p,q)$ and $\gamma(p,q)=\gamma(-p,-q)$. Computation of the semivariances $\gamma(p,q)$ and $\gamma(p,-q)$ is therefore sufficient. This analysis presumes that the surface is stationary (mean of zero). Therefore, linear trend in the surface must be removed. This is done by subtracting the mean plane, calculated by least-squares fitting of a first-order polynomial surface, from the DEM surface. Furthermore, it is generally recommended that the semivariogram be calculated only for lags up to half the series length (Klinkenberg 1994, Butler *et al.* 2001). This is considered as a maximum distance of reliability where the semivariance γ at a given lag (p,q) is sufficiently sampled (equation (1)).

Inspection of equation (1) shows that for a given (p,q) lag, the semivariance is evaluated along all parallel lines of direction ω on the surface thus giving a much bigger sample size than if a single elevation profile of the surface along direction ω had been used. Figure 2(*a*) shows an example semivariogram surface. These figures are best analysed by plotting extracted profiles on log–log axes. Figure 2(*b*) shows an example. It is important to note that plotting semivariance versus lag on log–log axes has the effect of damping high lag anisotropy. Here the profile has been extracted along the $0°$ direction corresponding to the p-lag component direction. The profile shows two linear sections with a break of slope. Each linear section corresponds to a scaling band within which the surface is self-affine, i.e. self-similar but with different scaling factors in different directions (Schroeder 1991). The existence of multiple bands on a given surface may be explained by the action of multiple processes, each at a different scale. For example, Robert (1988, 1991) attributed the observation of two scaling bands to grain and form roughness, respectively. Moreover, it should be noted that the number of scaling bands observed on a semivariogram profile is
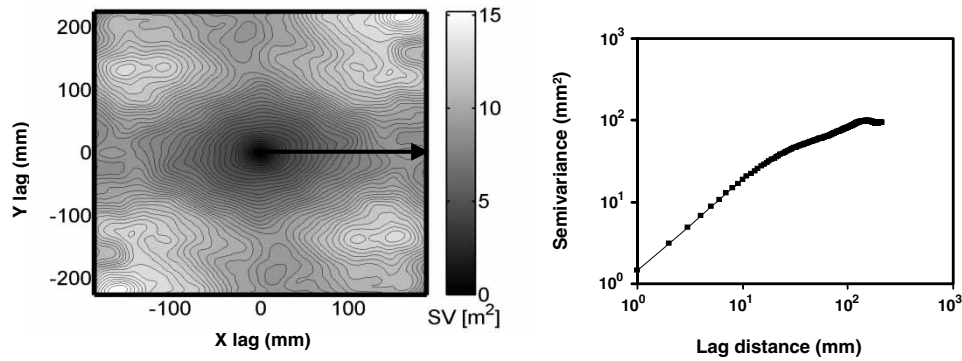
Figure 2. (*a*) Example of a semivariogram surface; (*b*) profile extracted from (*a*).

highly dependent upon the resolution and scale of the topographic data (profile or a surface) used in its calculation. Processes operating on a scale smaller than the resolution of the topographic data cannot be detected; those operating on a scale greater than the entire modelled surface or profile will remain inaccessible. However, the assumption that linear scaling bands are present in the surface gives a basis for an evaluation of external reliability. Provided the surface elevations may be fitted with a Gaussian distribution, derivations from linear behaviour may be attributed to errors in the surfaces or DEM, therefore allowing for evaluation of DEM quality without recourse to independent check data.

3. Methodology

3.1. *Data collection in the field*

For the purpose of this study, four gravel riverbed sites, labelled RSM1 through RSM4, were selected on the dried channel margins of the Ste-Marguerite river, Québec, Canada. The areas were selected for increasing roughness and grain size. Median diameter (D_{50}) for each site was evaluated as 18 mm, 27 mm, 57 mm and 61 mm respectively. Images were collected using a single Minolta X-300 35 mm film-based SLR camera, mounted on a gantry. The optical axis was always oriented to be approximately vertical. The camera could slide between two positions along an aluminium railing system. The translation (baseline) distance was calculated to obtain a 60% overlap in the stereo-pairs. The camera lens was approximately 1.1 m above the ground. Figure 3 shows raw images of all four study sites.

Within the overlap area of each stereo pair, 30 survey points were identified with targets. The targets consisted of copper discs of 1.5 cm diameter and approximately 2 mm thickness. Each target was painted in fluorescent orange and marked with a cross-hair. All targets were surveyed with a Leica TC-600 total station. To obtain better results, the standard total station prism staff was replaced by a prism mounted on a 15 cm steel prism-foot that finished in a sharpened point. Additionally, a level was added to the prism. No measure of camera exterior orientation parameters was taken in the field as these were determined during the processing stage.

3.2. *Digitization of images*

Digital images were obtained by scanning negatives to an interpolated density of 10 μm (2400 dpi) with 256 grey levels with a UMAX desktop scanner. One important feature of this scanner is the presence of two glass plates that flatten the

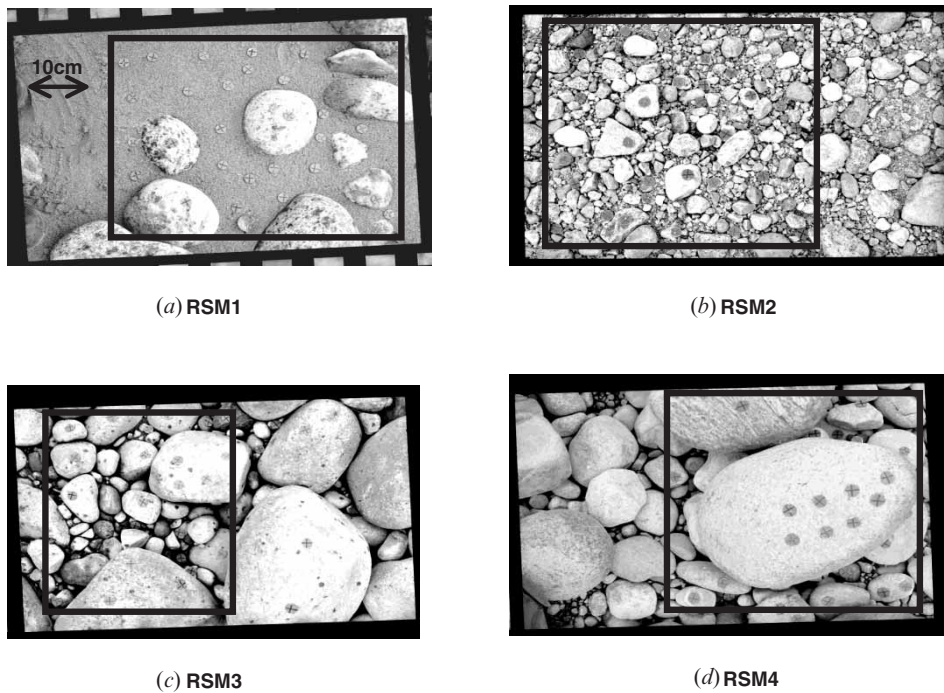(*a*) **RSM1**

(*b*) **RSM2**

(*c*) **RSM3**

(*d*) **RSM4**

Figure 3. Raw images of the four study sites. The areas within the frames are modelled by the DEMs.

film during scanning, therefore minimizing additional image deformation during this process. However, this is not a standard photogrammetric scanner and some loss of quality was expected to occur.

3.3. *Restitution of surface topography*

The stereo-pairs were processed using the OrthoMAX module of the ERDAS Imagine software. This softcopy photogrammetry package carries out interior orientation, ground control point measurement and estimates exterior orientation with a least-squares block bundle adjustment. At this point in the process, the CUBA software was used to perform camera calibration. With calibrated values for the camera parameters, automated DEM extraction may be carried out using area-based matching. The interior orientation is normally established using fiducial marks present on the image. In the case of a 35 mm SLR camera, such marks are absent and an alternative method must be applied. Short (1992) showed that, provided the inner geometry of the camera is stable and the dimensions of the negatives are known, the use of the corners of the negatives as fiducial marks were acceptable, giving rapid solutions for inner orientations with a minimal loss of accuracy. The image size was therefore set at 36 mm × 24 mm with fiducials in all four corners.

Ground control was established using 20 of the 30 survey targets, the other 10 being reserved as independent checkpoints. In the ground control measurement phase, the user must manually identify conjugate pairs for each ground control point. This will yield photo-coordinates for each ground control point used in camera calibration. Calibration is carried out with the CUBA software and requires initial values for camera principal distance (i.e. the focusing distance), principal point offset

and radial distortion. The initial value for camera principal distance was estimated using the basic lens equation (Wolf 1983) assuming a focal length of 50 mm and a flying height of 1.1 m. The parameters of principal point offset and lens distortion were initially set to zero. The CUBA software then carried a least-squares bundle adjustment to attempt to accurately estimate the camera parameters.

DEM collection was carried out with these calibrated camera parameters. During collection, several parameters may be user specified to control and optimize stereo matching performance. The parameters adopted here were determined by Butler *et al.* (1998) as being optimal for close-range digital photogrammetry of coarse gravels. The DEMs were collected at a spatial resolution of 1 mm yielding DEMs of approximately 500×500 pixels in size. Collection of 250 000 regularly spaced total station points, for each study site, would clearly not have been feasible.

3.4. *Assessment of data quality*

The first quality check was made by visual inspection. Comparison of DEMs and orthorectified images provided a qualitative measure of the overall success of the DEM in representing the topography of interest. Gross errors were identified as spikes in the DEM that are not present in the surface topography.

Quantitative aspects of DEM quality were examined in terms of random error, systematic error and external reliability. The quality of the block bundle adjustment was estimated with the standard deviation of unit weight parameter ($\hat{S}_w$). For cases where $\hat{S}_w < 1$, the problem is under-constrained and where $\hat{S}_w > 1$, the problem is overconstrained. Although this parameter should ideally be unity, values ranging from 0.5 to 2 are considered acceptable (Vision International 1995). High $\hat{S}_w$ values occurred when gross field measurement errors are present. Once identified, these erroneous points were eliminated from the analysis.

After visual inspection, unused survey points were used to establish mean elevation differences and standard deviation of elevation differences to quantify random error and systematic error in the surface, respectively. External reliability was evaluated with respect to the scaling properties of the surface. Prior to the calculation of semivariograms for each DEM, minor editing was carried out to eliminate spikes along the edges of the DEM. These errors may be dismissed as edge effects and should be eliminated since they have a great effect on the semivariogram (equation (1)). Thus, a local statistical filter with a spatial extent of 3×3 mm was applied locally to replace edge spikes by the local average. After editing, the semivariogram was computed for each DEM. Following Klinkenberg (1994) and Butler *et al.* (2001) a distance of reliability of half the image size was adopted. Therefore, each semivariogram was computed (equation (1)) with all combinations of p, ranging from 1 to $M/2$ and q ranging from $-N/2$ to $N/2$. Given the symmetry properties of equation (1), this was sufficient to obtain semivariances in all directions. The profiles extracted from the semivariogram surfaces were then examined to determine if the scaling properties were similar to those of natural surfaces.

4. Results

Repeated attempts at camera calibration with the CUBA software failed to provide reliable calibrated camera parameters. The principal point offset and radial distortion, were expected to be roughly constant in different images since the same camera was used. However, they showed variations of over 100%. Furthermore it was found that the error estimated by the calibration software for each parameter

was also of the order of 100%. Attempts at calibrating only the focal length were also inconclusive. The most likely reason for this failure is the presence of distortion in the image that was introduced by film curvature at the time of exposure. Film non-flatness at the time of exposure is often recognized as the major limiting factor for the successful calibration of non-metric cameras (Robson 1990, Fryer 1996).

DEMs generated with 20 control points and uncalibrated camera data were of an unexpectedly high quality. Figure 3 shows raw images for each study site; and figure 4 shows the corresponding DEMs. Feature identification is good, especially considering the fact that the camera data used in the process was approximate. The standard deviations of unit weight are, for sites RSM1 through RSM4, 1.26, 1.30, 1.10, 1.94, respectively. These results suggest that, for the scale of interest, full camera calibration may not be required.

It was decided to study the quality of DEMs generated with the uncalibrated and therefore approximate camera parameters to determine if these were of sufficient accuracy to yield geomorphologically meaningful information. Additionally, an analysis was carried out to determine the sensitivity of DEM quality to the number of control points. Thus, another series of DEMs was generated using uncalibrated camera data and an increasing number of control points. For each study site, additional DEMs were generated with three, five, ten and fifteen control points. Finally, a sensitivity analysis of the effect of a perturbation of the focal length was undertaken to assess the potential error introduced by the use of an approximate value for the camera focal length.
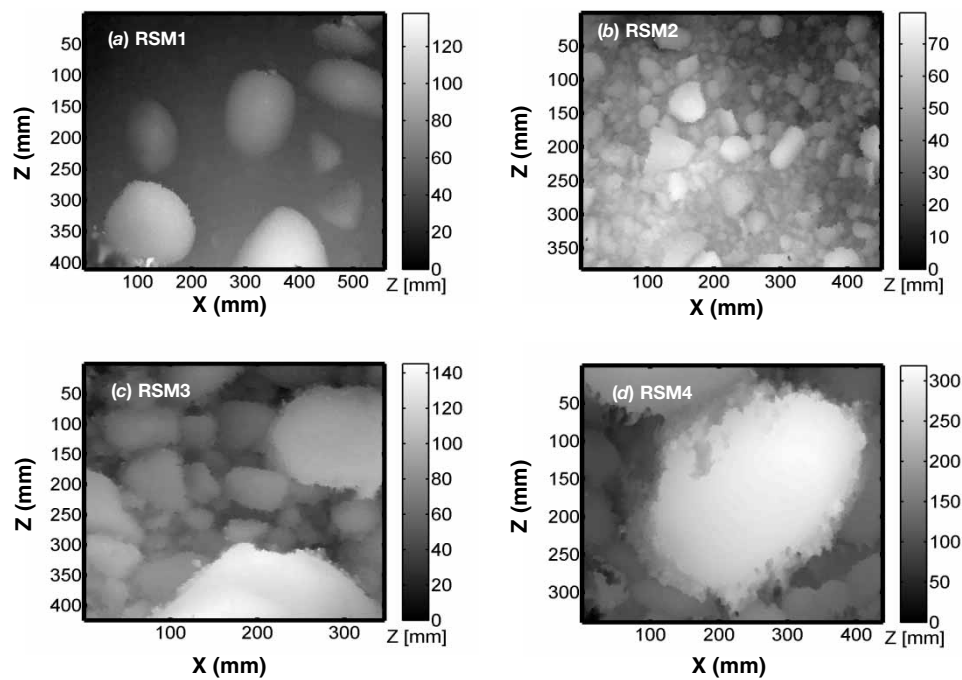

Figure 4.   Digital elevation models (DEMs) collected with 20 control points and uncalibrated camera parameters.

4.1. *Visual inspection of DEMs*

Figure 5 shows DEMs collected with three control points. The number of features identifiable in the DEM is immediately seen to be small with large areas showing significant levels of noise. This figure illustrates a well-established principle of photogrammetric design: the ground control points should cover the whole $X Y Z$ dimensions of the imaged surface. Particularly in figures 5(*a*) and 5(*b*), the top right and bottom left corners are of significantly reduced quality. An improved spread of control points could improve results and it is necessary to use more than the theoretical minimum of three ground control points (figure 5).

Figure 6 shows the DEMs collected with five control points. The increased coverage has led to a large increase in the level of feature identification. Increasing the number of control points beyond five had qualitatively little effect at first observation. However, if the 20-control-point DEMs (figure 4) and the five-control-point DEMs (figure 6) are subtracted it can be seen that stone edges are much more clearly defined in the 20 control point DEM (figure 7). This demonstrates that elevations in the vicinity of particle edges are more sensitive to the number of control points.

4.2. *Standard deviations of unit weight*

Table 1 gives $\hat{S}_w$ for all collected DEMs. It can be seen that for a small number of control points, the $\hat{S}_w$ tends to be below 1 meaning an under-constrained problem. However, results for 15 and 20 control points are well within the acceptable range of 0.5–2.
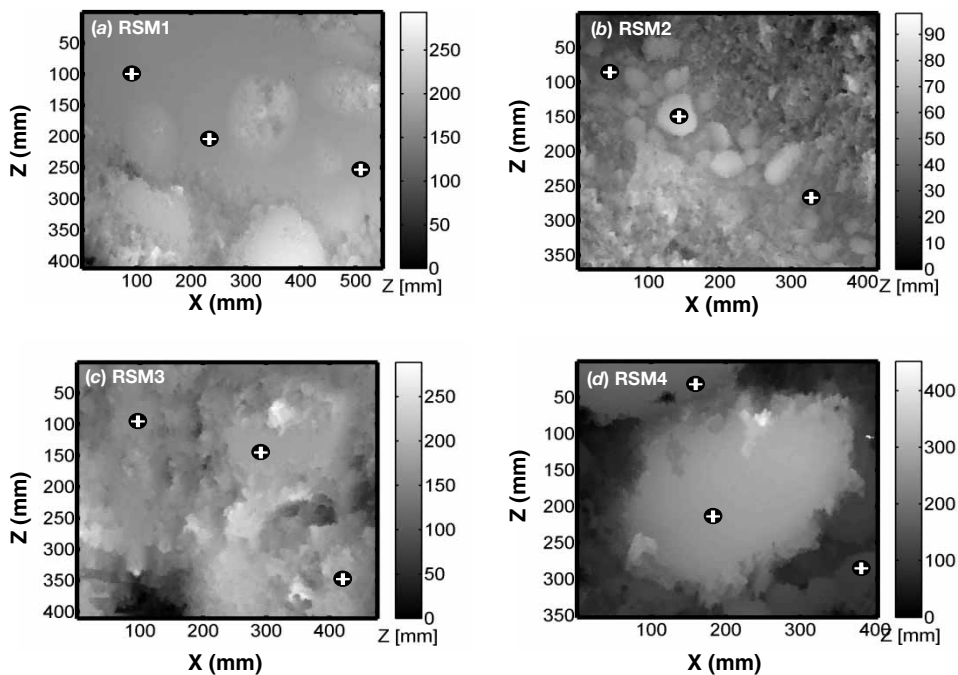

Figure 5.   Digital elevation models (DEMs) collected with three (shown with markers) control points and uncalibrated camera parameters.
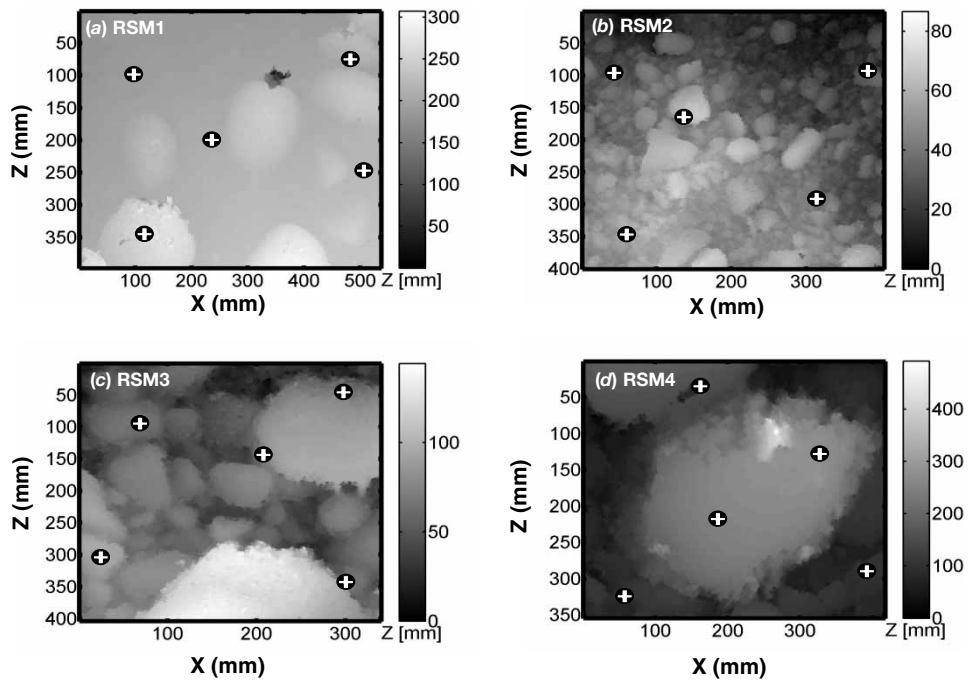
Figure 6. Digital elevation models (DEMs) collected with five control points and uncalibrated camera parameters.
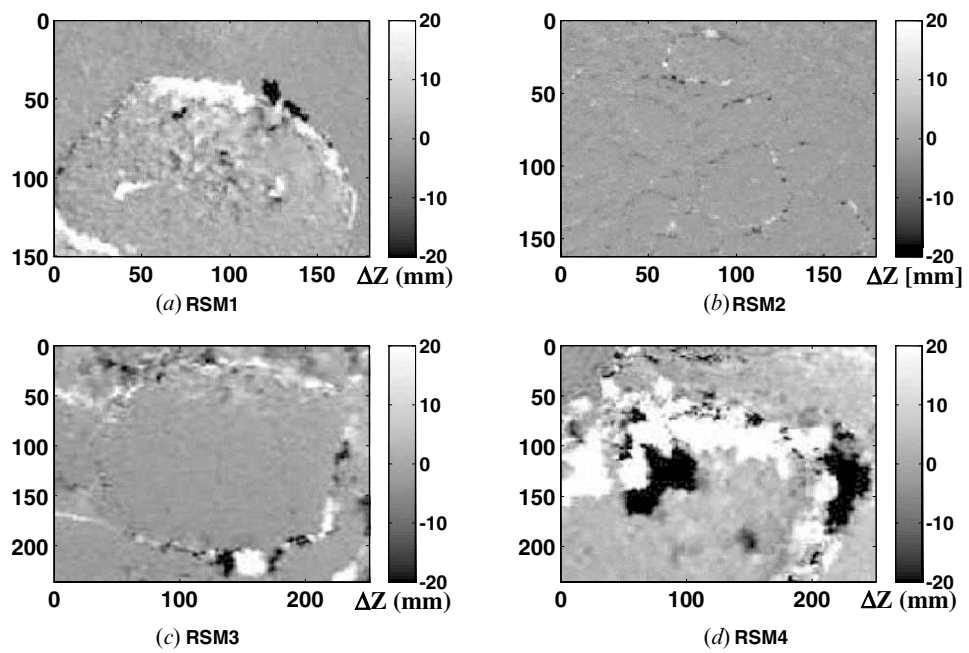

Figure 7. Enlarged areas showing the difference between the DEMs with 20 GCPs and 5GCPs.

Table 1. Standard deviations of unit weight.

	3GCP	5GCP	10GCP	15GCP	20GCP
RSM1	0.5	0.5	0.66	0.64	1.26
RSM2	0.69	0.55	1.16	1.19	1.30
RSM3	0.86	0.90	0.74	0.79	1.10
RSM4	0.70	0.85	1.20	1.33	0.94

4.3. *Independent check data analysis*

The unused surveyed targets were used as independent checkpoints for comparison with their elevations as predicted by the DEM. The mean difference of measured and predicted elevations and the standard deviation of this difference are normalized with the D_{50} value for each respective study site. Table 2 gives the results of this quality assessment. Surface systematic error is generally seen to be proportional to the number of ground control points, but with a large reduction in error in two cases with the increase to five control points. The trend for the standard deviation is less clear. The results for the 20GCP DEMs are nevertheless good. For all DEMs, the mean error for 20 control points is below 10% of the D_{50}. This yields mean surface errors from -1.5 mm to 3.6 mm. Similarly, the standard deviation of elevation differences for checkpoints yields surface precisions ranging from ± 2.1 mm to ± 8.5 mm. These results are encouraging since they are sub-centimetric, the required quality for this research. However, these results were generated with a small number of checkpoints offering limited spatial coverage of the surface, and further analysis is required to assess the quality of these DEMs.

4.4. *Matching precision*

Sites RSM1 and RSM2 are seen to have the highest percentage of matched points (table 3). These surfaces are the most textured and the stereo-matching algorithm

Table 2. Quality assessment based on elevation differences between independent checkpoints and DEM elevations. All values are expressed as a percentage of the D_{50} for the DEM surface.

Number of GCPs	RSM1		RSM2		RSM3		RSM4	
	mean (%)	std (%)	mean (%)	std (%)	mean (%)	std (%)	mean (%)	std (%)
3	-27.2	9.8	-19.8	19.4	-28.1	55.3	8.9	12.7
5	-27.8	11.5	-5.3	7.9	4.1	25.5	10.0	20.7
10	-20.4	13.0	-3.2	7.8	1.2	37.1	8.7	10.5
15	-16.7	11.5	0.4	8.2	2.9	21.6	6.2	11.6
20	-8.0	13.1	0.0	8.1	7.2	18.4	5.0	17.7

Table 3. Percentage of matched points.

	3GCP	5GCP	10GCP	15GCP	20GCP
RSM1	71	90	89	90	90
RSM2	55	78	74	82	71
RSM3	30	33	42	42	43
RSM4	47	48	48	55	55

will perform best on these. An examination of the spatial distribution of matched and interpolated points revealed that, for RSM1 and RSM2, matched points are fairly evenly distributed along the surface, but with perspective errors reflected in some concentrations of interpolated points along rock edges. In cases RSM3 and RSM4, the coarser grains have increased roughness and relief and have made the effects of perspective error more important. This is reflected in lower matching percentages. The increased grain sizes have increased the total area of the DEM that is subject to perspective error thus explaining the matching results.

4.5. *Scaling analysis*

External reliability, with respect to scaling properties of the surface, was evaluated using the semivariogram. Following editing, semivariogram surfaces were generated for each DEM with three and 20 control points. Figure 8 shows example semivariogram surfaces for RSM3. It can be seen that the three-ground-control-point case has larger semivariance and important differences in morphology. In order to assess the presence or absence of power law scaling behaviour, semivariogram profiles were extracted from the surface along the p lag component direction, as in figure 2, and plotted in log–log space (figure 9). Examination of profiles along other directions yielded no additional information pertaining to DEM quality. Figure 9 shows that the three-ground-control-point (3GCP) profiles have larger semivariance. Furthermore, the greatest differences are observed at smaller scales. Similarities may be seen between cases RSM1 and RSM4 and between RSM2 and RSM3. For cases RSM1 and RSM4, the large-scale section appears to have higher slope than the small-scale section. This is contrary to theoretical expectations and a plausible explanation would be that error at small lags is very important. Cases RSM2 and RSM3 fit more closely with theoretical predictions since slope at high lags is smaller than at lower lags. The differences in semivariogram profiles may be explained by differences in errors and how these errors affect the semivariogram. The large error at low lags for case RSM4 may be understood by re-examining figure 5(*d*). The large amount of small-scale noise present along rock edges dominates the semivariogram. Since a large amount remains in the 20GCP case (figure 4(*d*)), the semivariogram profiles are similar. Profiles for RSM1 may also be understood by re-examining the DEMs. The profiles show an important change in shape from concave to convex. An examination of the DEMs used in the generation of the semivariograms (figures 4(*a*)
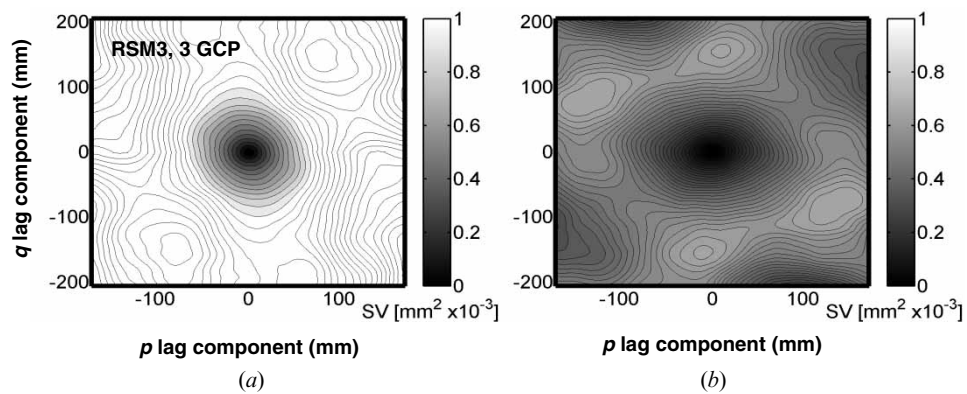

Figure 8.   Semivariogram surfaces for site RSM3. (*a*) 20GCP case; (*b*) 3GCP case.
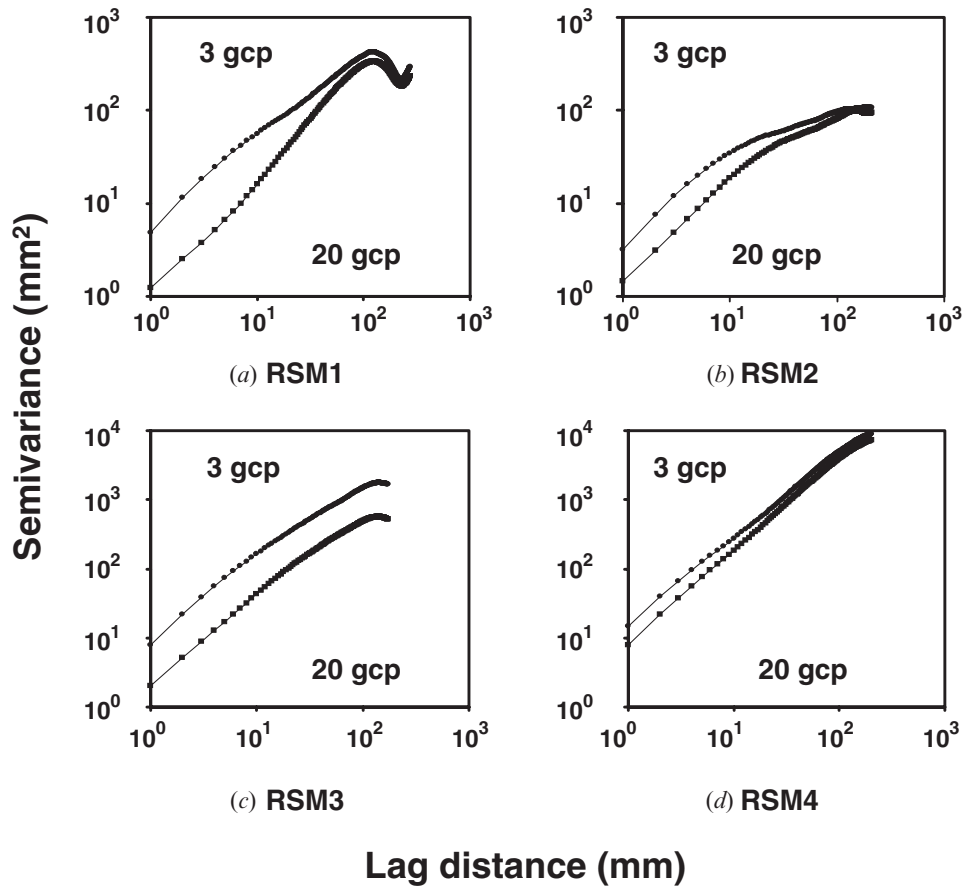
Figure 9.   Semivariogram profiles for 3 GCPs and 20 GCPs extracted along the *p* lag axis.

and 5(*a*)) show the errors to be of a different nature. In the 3GCP case (figure 5(*a*)) large areas with small amplitude error ('noise') can be seen. However, in figure 4(*a*) the errors seem to be located in a few small areas, particularly along the edge of rocks. These spikes around rock edges were not edited and these results suggest that they adversely affect the semivariogram by causing an over-estimation of semi-variance at small lags. This means that the errors in the 3GCP case are related to problems in the 3D restitution of the surface caused by insufficient control points. However, for the 20GCP case, the errors are controlled by perspective problems which is why error zones are found along rock edges.

Quantitative analysis of semivariogram profiles was based on their linearity. Prior to calculating the linearity of the profiles, the user must establish slope breaks between self-affine scaling bands. Slope breaks were identified visually with a graphic interface running under the MATLAB environment. The user must determine the number of segments and then visually regress lines drawn across the points of each segment. Break points are then given by line intersections. Once slope breaks are established, linear regression is carried out on each segment and the sum of squared errors (SSE) is used to quantify linearity. Table 4 gives the results of the linearity tests. For sites RSM2, RSM3 and RSM4, the addition of control points has linearized

Table 4. SSE values for linear regressions carried out on scaling bands.

Number of GCPs	RSM1 SSE		RSM2 SSE		RSM3 SSE		RSM4 SSE	
	band 1	band 2	band 1	band 2	band 1	band 2	band 1	band 2
3	1.9×10^{-1}	n.a.	7.6×10^{-2}	1.2×10^{-3}	5.7×10^{-2}	8.4×10^{-3}	2.2×10^{-2}	1.0×10^{-3}
20	2.3×10^{-1}	n.a.	3.5×10^{-4}	8.1×10^{-3}	1.1×10^{-2}	6.2×10^{-3}	7.4×10^{-3}	5.8×10^{-2}

the first band of the semivariogram profile. In the case of RSM1, the curvature in the small-lag section suggests that further editing is required in order to obtain the expected linear behaviour. It can therefore be seen that the addition of control points produces a DEM that obeys more closely the power-law scaling pattern recognized in natural surfaces. However, this analysis also suggests that more research is required to fully understand the effect of error on the scaling properties of a surface.

4.6. *Sensitivity to focal length error*

Given the difficulties of determining an adequate camera calibration, an analysis was undertaken to examine the effect of an approximate focal length upon derived DEMs. A perturbation of 2 mm was used representing a change of approximately 50 cm in object space. This is a major perturbation that exceeds the error associated with manual measurement of the focusing distance with a steel tape. For the 20GCP DEM of each study site, this 2 mm perturbation was applied to the focal length and the DEM was recollected. Once again, edge effect spikes were edited prior to comparison in both perturbed and non-perturbed DEMs.

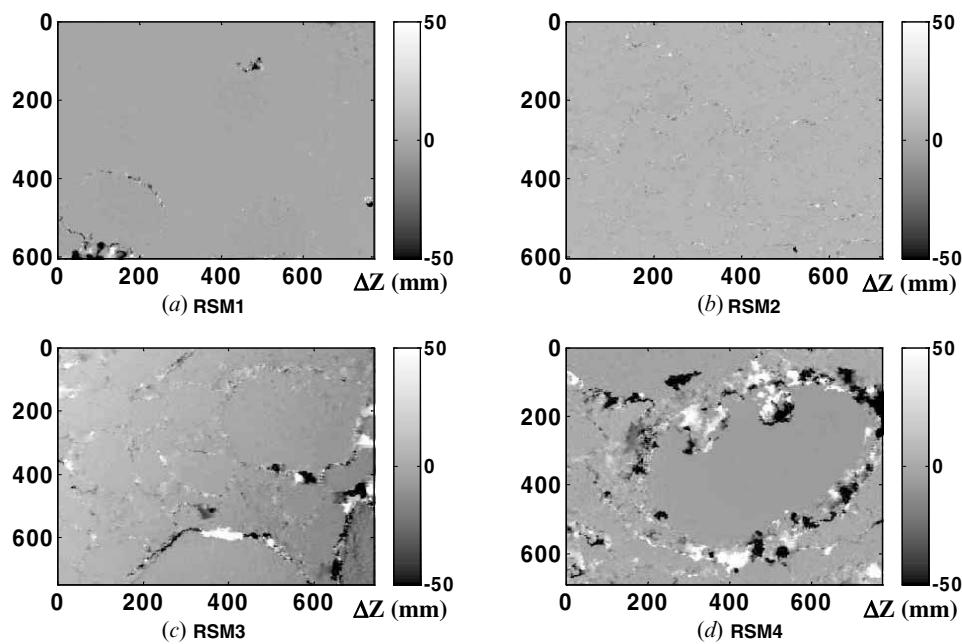The resulting DEMs were compared with the original 20GCP DEM (figure 10).

Figure 10. DEM differences for focal length perturbation results.

It can be seen that only a few points show a large difference in elevation. Furthermore these points are almost exclusively located along rock edges where perspective errors are very important and the collection process is unstable. Overall the median differences, expressed as a percentage of D_{50} are -0.1%, -0.1%, -0.3% and -1.3% for sites RSM1 through RSM4, respectively. This result demonstrates that areas of perspective problems are more sensitive to focal perturbation since coarser substrates generally have more relative relief and thus are more subject to perspective problems. Although there is a trend for the perturbed DEM to be slightly higher, the difference in elevation remains very small when compared to the requirements of the study. However, it was noted that the block bundle adjustment in OrthoMAX compensated for focal length perturbations by adjusting the camera flying height. During this free-network least-squares adjustment, the coordinates of the ground control points are considered fixed and therefore the adjustment varies other parameters to obtain a solution. This explains why focal perturbation has such a minor effect. It also indicates why successful DEM collection was possible despite continued uncertainties associated with camera interior orientation.

5. Discussion

The objective of this study was to develop a cost-effective non-metric digital photogrammetry methodology capable of sub-centimetric spatial resolution and surface precision. Statistics for the 20GCP DEMs show that the required sub-centimetric precision was achieved. Scaling analysis reveals the expected power-law behaviour, thus supporting the validity of the DEMs. Matching statistics were lower than hoped for, but some loss of quality is inevitable when using non-calibrated cameras. Furthermore, in coarse environments poorer performance of the matching algorithm is expected due to the increased presence of perspective problems. However, the overall results suggest that camera calibration is not required in order to obtain sub-centimetre precision at this scale. Assuming a camera height of 110 cm and an average surface precision of 0.5 cm, this represents an error of 1/220. Whilst obtaining smaller errors could be possible using advanced methods and specialized equipment, this was not necessary. The loss of accuracy is offset by gains of accessibility and cost-effectiveness.

Having numerous and well-surveyed ground control was the key element in the success of this methodology. This research showed that 15 to 20GCPs are necessary in order to eliminate camera calibration. Accurate ground control was also found to be highly important. Initial attempts at photogrammetric surveys in the course of this research have shown that inaccurate ground survey will lead to very low DEM quality and may even prevent the block bundle adjustment from converging thus making DEM collection impossible. One key element was found to be prism foot design. Since ground control targets are small, it is imperative to accurately place the prism on a given target. Conventional total station rods were found to be awkward and inaccurate for this scale of work. Positioning of ground control is also important. Figure 3 shows that when control points are poorly aligned, a loss of DEM quality occurs. Control points should be distributed evenly through the X, Y and Z dimensions of the study site.

Perspective errors are the most important cause of matching failure and DEM error. Unfortunately, perspective errors are a fundamental difficulty for photogrammetry where there is high relative relief, area-based matching stereo-matching algorithms will always achieve poor results in these areas. Post-processing provides

the only solution. Automated DEM collection requires a post-processing phase of inspection and manual editing to a greater extent than traditional manual DEM collection methods. Gross errors can easily be identified and replaced by the local average. Smoothing is commonly applied to DEMs. However recent results show that simple automated editing using a 3×3 low-pass filter may cause curvature in the semivariogram profile. This suggests that more refined filter design is required if DEMs are to retain the power-law scaling behaviour characteristic of natural surfaces. One possible avenue of research is in the design of filtering methods that target areas of perspective error.

6. Conclusions

A method has been proposed for cost-effective implementation of digital photogrammetry. In close-range applications, the resulting surface precision of 1:220 obtained with 'off the shelf' equipment translates into sub-centimetric surface precision. This level of precision, achieved without camera calibration, is made possible by the presence of numerous and redundant ground control points. Issues of data quality still require more research in order to be properly assessed. Scaling analysis offers much potential for establishing a measure of DEM quality without recourse to large check datasets. However, these results show that different types of errors, present in an automatically collected DEM, will affect the semivariogram in different ways. Progress in this area therefore requires research and classification of the possible ways in which errors affect the scaling properties of a DEM. Current methods of assessment still produce a valid estimate of DEM quality. Therefore the results show that photogrammetry can be made accessible to a much wider range of users who might benefit from high-density topographic data with reasonable accuracy obtained at minimal cost.

References

AHMAD, A., and CHANDLER, J. H., 1999, Photogrammetric capabilities of the Kodak DC40, DCS420 and DCS460 digital cameras. *Photogrammetric Record*, **16**, 601–615.

BERGERON, N. E., 1998, Scale-space analysis of stream-bed roughness in coarse gravel-bed streams. *Mathematical Geology*, **28**, 537–561.

BUTLER, J. B., LANE, S. N., and CHANDLER, J. H., 1998, Assessment of DEM quality for

characterising surface roughness using close range digital photogrammetry. *Photogrammetric Record*, **16**, 271–291.

BUTLER, J. B., LANE, S. N., and CHANDLER, J. H., 2001, Characterisation of the structures of river-bed gravels using two-dimensional fractal analysis. *Mathematical Geology*, **333**, 301–330.

CHANDLER, J. H., and PADFIELD, C. J., 1996, Automated digital photogrammetry on a shoestring. *Photogrammetric Record*, **15**, 545–559.

CHANDLER, J. H., 1999, Effective application of automated digital photogrammetry for geomorphological research. *Earth Surface Processes and Landforms*, **24**, 51–63.

COOPER, M. A. R., and CROSS, P. A., 1998, Statistical concepts and their application in photogrammetry and surveying. *Photogrammetric Record*, **12**, 637–663.

CUNJAK, R. A., 1988, Behaviour and microhabitat of young Atlantic salmon (*salmo salar*) during winter. *Canadian Journal of Fisheries and Aquatic Sciences*, **45**, 2156–2160.

DOWMAN, I. J., 1996, Fundamentals of digital photogrammetry. In *Close Range Photogrammetry and Machine Vision*, edited by K. B. Atkinson, Caithness-Whittles, Scotland, pp. 52–77.

FRYER, J. G., 1996, Camera calibration. In *Close Range Photogrammetry and Machine Vision*, edited by K. B. Atkinson, in press, pp. 156–179.

GREGORY, J. S., and GRIFFITH, J. S., 1996, Winter concealment by subyearling rainbow trout: space size selection and reduced concealment under surface ice and in turbid water conditions. *Canadian Journal of Fisheries and Aquatic Sciences*, **74**, 451–455.

HEGGENES, J., 1996, Habitat selection by brown trout (*salmo trutta*) and young Atlantic salmon (*s. salar*) in streams: static and dynamic hydraulic modelling. *Regulated Rivers: Resource Management*, **12**, 155–169.

KLINKENBERG, B., 1994, A review of methods used to determine the fractal dimension of linear features. *Mathematical Geology*, **26**, 23–46.

LANE, S. N., CHANDLER, J. H., and PORFIRI, K., 2001, Monitoring flume channel surfaces using automated digital photogrammetry. *ASCE Journal of Hydraulics*, **12 710**, 871–877.

LANE, S. N., JAMES, T. D., and CROWELL, M. D., 2000, Application of digital photogrammetry to complex topography for geomorphological research. *Photogrammetric Record*, **16**, 793–821.

NIKORA, V. I., GORING, D. G., and BIGGS, B. J. F., 1998, On gravel-bed roughness characterization. *Water Resources Research*, **34**, 517–527.

RIMMER, D. M., PAIM, U., and SAUNDERS, R. L., 1983, Changes in the selection of microhabitat by juvenile Atlantic salmon (*salmo salar*) at the summer–autumn transition in a small river. *Canadian Journal of Fisheries and Aquatic Sciences*, **41**, 469–475.

ROBERT, A., 1988, Statistical properties of sediment bed profiles in alluvial channels. *Mathematical Geology*, **20**, 205–225.

ROBERT, A., 1991, Fractal properties of simulated bed profiles in coarse-grained channels. *Mathematical Geology*, **23**, 367–382.

ROBSON, S., 1990, The physical effects of film deformation in small format camera calibration. *International Archives of Photogrammetry and Remote Sensing*, **29**, 561–567.

RUSS, J. C., 1994, *Fractal Surfaces* (New York: Plenum Press).

SCHROEDER, M. R., 1991, *Fractals, Chaos, Power Laws: Minutes from an Infinite Paradise* (New York: Freeman Press).

SHORT, T., 1992, The calibration of a 35 mm non-metric camera and the investigation of its potential use in photogrammetry. *Photogrammetric Record*, **14**, 313–322.

SHORT, T., 1999, 'How to use CUBA, the City University Bundle Adjustment' software and web document available at: www.acts.demon.co.uk.

STOJIC, M., CHANDLER, J. H., ASHMORE, P., and LUCE, J., 1998, The assessment of sediment transport rates by automated digital photogrammetry. *Photogrammetric Engineering and Remote Sensing*, **64**, 387–395.

VISION INTERNATIONAL, 1995, *IMAGINE OrthoMAX User's Guide*.

WALKER, J. P., and WILLGOOSE, G. R., 1999, On the effect of digital elevation model accuracy on hydrology and geomorphology. *Water Resources Research*, **35**, 2259–2268.

WELSH, R., and JORDAN, T. R., 1983, Analytical non-metric close-range photogrammetry for monitoring stream channel erosion. *Photogrammetric Engineering and Remote Sensing*, **49**, 367–374.

WOLF, P. R., 1983, *Elements of Photogrammetry*, 2nd edn (New York: McGraw-Hill).